3.1.5 Attrition, Activity and Selectivity Characteristics of Supported Iron Fischer-Tropsch Catalysts

Introduction

Iron catalysts undergo a series of phase changes during activation and use in the Fischer-Tropsch synthesis (FTS) (1,2) which cause the volume of catalyst particles to change. These volume changes can cause stresses to develop within individual particles and within agglomerations of catalyst particles which may ultimately cause attrition. The following description utilizes the bulk properties for iron oxide and iron carbide compounds (3-7).

Using the densities listed in Table 1, the volume changes that occur upon activation of an iron catalyst that starts as Fe_2O_3 are shown in Table 2. The initial reduction of Fe_2O_3 to Fe_3O_4 results in a small (2%) decrease in volume and should not induce much stress upon individual catalyst particles nor upon catalyst agglomerates. The next potential step in the reduction, if it occurs, and to date there is no definitive evidence that FeO does form in significant quantities, leads to a 18.9% volume decrease. The conversion to Fe_3C results in a further decrease in volume by 35%, and a similar decrease if Fe_5C_2 is formed. Thus, overall the activation process results in a decrease in the volume of the individual catalyst particle; this decrease in volume may or may not be transferred to the catalyst agglomerate.

During use, some fraction of the iron carbide is converted to Fe_3O_4. The conversion of Fe_3C to Fe_3O_4 results in an increase in volume of 91%, and a similar increase for Fe_5C_2. The reoxidation step therefore has the potential to induce severe strains on the individual catalyst particle and upon the catalyst agglomerate. Thus,

there is potential for the reoxidation step to provide the stress to cause the formation of catalyst fines during operation with the iron catalyst.

Catalyst attrition is a major problem in the operation of slurry phase FT reactors using iron-based catalysts (8, 9). During slurry phase FTS with bubble column reactors, catalysts are generally separated from accumulated reactor wax by either internal filtration or an external settling system which circulates catalyst back to the reactor. Catalyst fines produced by attrition may cause filters to plug and are difficult to separate by settling. The problem of attrition is even more pronounced when bench scale continuous stirred tank reactors (CSTR) are used. The impeller of the CSTR greatly increases the rate of attrition which makes it very difficult to test catalysts which produce a large amount of wax. Precipitated iron catalysts with low wax yields (C_{12}+ < 30 wt%) have been operated in a CSTR for over 3000 hours in our laboratory. We have found that a 0.5 µm sintered metal filter can remove accumulated reactor wax at a faster rate than it is produced despite catalyst attrition. On the contrary, high wax producing catalysts (C_{12}+ > 60 wt%) usually cannot be run for longer than 200 to 500 hours (depending on catalyst loading) because the high rate of wax production overwhelms the filters if catalyst fines are present. We have also observed that cobalt catalysts supported on alumina can be operated for extended time even in a high wax producing mode. Scanning electron microscopy of these supported cobalt catalysts showed that attrition was minimal. As a result we decided to test the attrition of supported iron catalysts.

A logical route to the development of a robust FTS catalyst, that can be easily separated from reactor wax, is to employ an attrition resistant support. In general, supported iron catalysts have been considered to be inferior to precipitated iron

catalysts because of strong interactions between iron and the most commonly used supports: alumina and silica (1). To neutralize the acidity of silica and alumina, a large amount of alkali promoter (potassium) must be used to achieve reasonable alkene selectivity and low methane yield. Unfortunately a consequence of using a high level of potassium is that stability is generally poor (1). In addition, a loss of FTS activity may occur if iron reacts with the support to form an inactive species such as iron silicates or $Fe_xAl_{3-x}O_4$ mixed spinels. The reaction of alumina with iron can be prevented by using an aluminate as a support. Toledo et al. have studied the dehydrogenation of 1-butene with iron supported on zinc aluminate and with $ZnFe_xAl_{2-x}O_4$ mixed spinels (10). They found that the supported catalyst was the most active because iron was located in octahedral vacancies on the surface of the $ZnAl_2O_4$ support and did not migrate into the bulk of the support to form $ZnFe_xAl_{2-x}O_4$ species. As part of our effort to develop a robust FTS catalyst, we have prepared a series of catalysts containing 20 weight percent iron on silica, magnesium silicate, alumina and magnesium aluminate. Reported herein are the activity, selectivity and attrition properties of these catalysts used in the slurry phase FTS with a CSTR.

Experimental

Catalyst Preparation

Four supports were impregnated with $Fe(NO_3)_3 \cdot 9H_2O$, $Cu(NO_3)_2 \cdot 3H_2O$ and KNO_3. The supports used were silica (Grace), alumina (Discovery Chemicals), magnesium silicate (Fisher) and magnesium aluminate. The silica, alumina and magnesium aluminate supports were screened to 60-325 mesh and the magnesium silicate was used as received, 60-100 mesh. Silica, alumina and magnesium silicate were activated at 600^{o}C for 4 hours. Magnesium aluminate was prepared by coprecipitating Mg-Al

hydroxides from $Mg(NO_3)_2 \cdot 6H_2O$ and $Al(NO_3)_3 \cdot 9H_2O$ (1:2 molar ratio) followed by calcination at 400°C for 16 hours and 800°C for an additional 16 hours.

The typical impregnation procedure was as follows. The support (86 g) was heated to 100°C while $Fe(NO_3)_3 \cdot 9H_2O$ (125 g), $Cu(NO_3)_2 \cdot 3H_2O$ (3.96 g) and KNO_3 (3.61 g) were melted in an oil bath at 70°C. The melt was slowly added to the support with good mixing. The impregnated support was then calcined at 300°C for 2 hours. The impregnation and calcination procedures were repeated resulting in a catalyst with approximately 21-23 wt% Fe. X-ray diffraction showed the crystalline phase to be α-Fe_2O_3 for all four catalysts (Figure 1). Nominal compositions and BET data for the supports and catalysts are shown in Table 3.

FTS conditions

Approximately 40 g of catalyst and 290 g of Ethylflo 164 oil (C_{30}) were loaded into one liter stirred autoclave reactors. The slurry was treated with hydrogen at 120 L h^{-1} (referenced to 0°C, 0.10 Mpa) at ambient pressure and the temperature was increased to 270°C at 120°C h^{-1}. Hydrogen reduction was carried out for 24 h and then the temperature was lowered to 250°C. The pressure was increased to 1.31 MPa and a catalyst sample was taken. Carbon monoxide flow was started and the hydrogen flow gradually decreased until the total flow rate was 3.1 SL h^{-1}g-Fe^{-1} and the H_2/CO ratio was 0.7. Additional catalysts samples were withdrawn at ~100 h and at the end of the runs. Catalyst samples were Soxhlet extracted to remove accumulated wax and were analyzed by scanning electron microscopy (SEM).

Results and Discussion

Carbon monoxide conversion for each supported catalyst is shown in Figure 2. The 100Fe/6.0Cu/8.1K/250Al_2O_3 and 100Fe/6.0Cu/8.0K/260$MgAl_2O_4$ catalysts had the

highest conversions. Both went through a long induction period in which the conversion increased from ~40% to 60%. A reactor upset occurred during the 100Fe/6.0Cu/8.1K/250Al_2O_3 run in which the hydrogen flow was cut off for 2-8 hours; however, within 72 hours the conversion had recovered. The 100Fe/6.0Cu/8.1K/250SiO_2 and 100Fe/6.0Cu/8.1K/260MgO·7.5SiO_2 catalysts had maximum carbon monoxide conversions of 32% and 7%, respectively and had poor stability. Hydrocarbon production rates are compared to a precipitated iron catalyst containing similar potassium and copper (100Fe/3Cu/8K/5SiO_2) in Figures 3 and 4. The 100Fe/6.0Cu/8.1K/250Al_2O_3 and 100Fe/6.0Cu/8.0K/260$MgAl_2O_4$ catalysts both had maximum values >0.35 g h^{-1}g-Fe^{-1} while the 100Fe/6.0Cu/8.1K/250SiO_2 and 100Fe/6.0Cu/8.1K/260MgOxSiO_2 catalysts were somewhat lower at 0.2 and 0.05 g h^{-1}g-Fe^{-1}, respectively. The low activity of the magnesium silicate supported catalyst is probably due to sulfur poisoning; elemental analysis of the magnesium silicate showed 0.3 weight percent sulfur. The precipitate 100Fe/3Cu/8K/5SiO_2 catalyst had a hydrocarbon production rate over 0.5 g h^{-1}g-Fe^{-1}, so the best supported catalyst had FTS activity roughly 75% that of the precipitated catalyst on a iron mass basis. In terms of catalyst mass (Figure 4), the precipitated catalyst was much more active than the supported catalsyts.

The induction period seen with the alumina and magnesium aluminate supported catalysts is typical of catalysts that are not reduced adequately during the activation procedure. Thermogravimetric analysis of the four catalysts is shown in Figure 5. Reduction in hydrogen showed two steps corresponding to: (1) α-$Fe_2O_3 \rightarrow Fe_3O_4$ and (2) $Fe_3O_4 \rightarrow Fe$. The first step (278-329^oC) was exothermic while the second (483-510^oC) was slightly endothermic. The presence of magnesium lowered the first

reduction step temperature; however, no effect was seen on the second step. Both reduction steps occurred at lower temperature for silica supported catalysts than alumina supported catalysts. Based on these data an activation temperature higher than 270^{o}C might improve the activity.

Methane, alkene and 1-alkene selectivities have been compared to the precipitated 100Fe/6Cu/8K/6SiO_2 catalyst. Methane selectivity (Figure 6) as a function of time on stream increased in the following order for the different supports: $MgAl_2O_4$ (<5%) < Al_2O_3 (5-6%) < SiO_2 (>8%) < MgO-3.75SiO_2 (9-15%); however, the best supported catalyst had significantly higher methane yield than precipitated catalyst (~3%). Alkene selectivity as a function of carbon number for the SiO_2, Al_2O_3 and $MgAl_2O_4$ supported catalysts is shown in Figure 7. Alkene selectivity was similar for all supported catalysts except the $MgAl_2O_4$ supported catalyst had much higher ethylene selectivity than all other catalysts. The ratio of 1-alkene to total alkene as a function of carbon number is shown in Figure 8. The SiO_2 supported catalyst produced slightly more internal alkenes than the Al_2O_3 and $MgAl_2O_4$ supported catalysts indicating that SiO_2 catalyzes alkene isomerization. The precipitated catalyst had higher alkene and 1-alkene selectivity than any of the supported catalsyts and in general, the alkene and 1-alkene selectivity decreased with increasing carbon number much more rapidly for the supported catalsyts than for the precipitated catalyst. Product distributions for the SiO_2, Al_2O_3 and $MgAl_2O_4$ supported catalysts are compared to the precipitated catalyst in Table 4. In general, the supported catalysts produced a lighter product than the precipitated catalyst. The C_{12}+ selectivity decreased in the order: precipitated (65 wt.%) > $MgAl_2O_4$ (54%) > Al_2O_3 (42%) > SiO_2 (34%). Overall, the selectivity and activity of the $MgAl_2O_4$ supported catalyst is the most similar to the precipitated catalysts.

The main purpose for running these catalysts was to develop a catalyst resistant to attrition in a continuous stirred tank reactor. Scanning electron micrographs of the four supported catalysts before FTS and after FTS are shown in Figures 9 and 10. All catalysts had particle sizes ranging from 250 to 60 µm before FTS. The MgO-3.75SiO_2 supported catalyst showed no signs of attrition; particle size and shape were the same before and after FTS. The SiO_2 supported catalyst showed little signs of attrition; the particle size remained unchanged; however, the sharp edges of the particles evident before FTS were smoothed by the end of FTS. The Al_2O_3 and $MgAl_2O_4$ supported catalysts were not as attrition resistant as the SiO_2 and MgO-3.75SiO_2 supported catalysts; both catalysts had fractured into smaller particles. After 312 hours of FTS the Al_2O_3 supported catalyst consisted of particles between 30 and 100 µm. The $MgAl_2O_4$ supported catalyst broke up into less than 30 µm particles after 264 hours of FTS; however, this attrition is not nearly as severe as encountered with precipitated iron catalysts. Despite the attrition seen with the $MgAl_2O_4$ supported catalyst, wax-catalyst separation was still possible.

It is clear from these data that alumina and $MgAl_2O_4$ supported catalysts have superior activity and selectivity than SiO_2 and MgO-3.75SiO_2 supported catalysts. The best activity and selectivity was obtained with the $MgAl_2O_4$ supported catalyst; however, it was substantially inferior to a comparably promoted precipitated iron catalyst. All of the supported catalysts studied showed much better attrition characteristics than precipitated iron catalysts; the SiO_2 and MgO-3.75SiO_2 supported catalysts showed very little attrition even in the harsh environment of a CSTR.

References

1. M. E. Dry, in: *Catalysis-Science and Technology*, Vol. 1, eds. J. R. Anderson and M. Boudart (Eds), Springer, Berlin, 1981) ch. 4.
2. R. J. O'Brien, L. Xu, D. R. Milburn, Y.-X. Li, K. J. Klabunde, and B. H. Davis, *Topics in Catal.* **2,** 1, (1995).
3. X-ray diffraction data (39-1088).
4. Natl. Bur. Std. Monogr. **25**, 1837 (1981).
5. Natl. Bur. Std. Monogr. **25**, 531 (1967).
6. Natl. Bur. Std. Monogr. **25**, 2172 (1985).
7. L. J. E. Hofer, E. M. Cohn, and W. C. Peebles, *J. Am. Chem. Soc.* **71**, 189 (1949).
8. B. Jager, R. Espinoza, *Topics in Catal.* **23**, 17 (1995).
9. R. Srinivasan, L. Xu, R. L. Spicer, F. L. Tungate, and B. H. Davis, *Fuel Sci. Techn. Int.* **14**, 10 (1996).
10. J. A. Toledo, M. A. Valenzuela, H. Armendáriz, G. Aguilar-Ríos, B. Zapata, A. Montoya, N. Nava, P. Salas, and I. Schifter, *Catal. Lett.* **30**, 279 (1995).

Table 1
Densities of Iron Oxides and Carbides which may be Present During Activation and Fischer-Tropsch Synthesis

Compound	Density	Vol/g	Equivalent Vol/g Fe
FeO[a]	5.97 g/cm^3	0.1675 cm^3/g	0.2155 cm^3/g Fe
α-Fe_2O_3[b]	5.27 g/cm^3	0.1898 cm^3/g	0.2714 cm^3/g Fe
Fe_3O_4[c]	5.20 g/cm^3	0.1923 cm^3/g	0.2658 cm^3/g Fe
Fe_3C[d]	7.684 g/cm^3	0.1302 cm^3/g	0.1395 cm^3/g Fe
Fe_5C_2[e]	7.672 g/cm^3	0.1303 cm^3/g	0.1416 cm^3/g Fe

a. X-ray diffraction data (39-1088).
b. *Natl. Bur. Std. Monogr.*, **25**, 1837 (1981).
c. *Natl. Bur. Std. Monogr.*, **25**, 531 (1967).
d. *Natl. Bur. Std. Monogr.*, **25**, 2172 (1985).
e. Hofer et al., *J. Am. Chem. Soc.,* **71**, 189 (1949).

Table 2
Oxidation Reduction Steps which may Occur During Activation and Subsequent Oxidation of Iron Fischer-Tropsch Catalysts

Compound	Volume, cm^3/g Fe	Volume Change, cm^3/g Fe (%)
Fe_2O_3	0.2714	
↓	↓	
Fe_3O_4	0.2658	+0.0056 (-2.06%)
↓	↓	
FeO	0.2155	-0.0503 (-18.9%)
↓	↓	
Fe_3C	0.1395	-0.0076 (-35.3%)
↓	↓	
Fe_3O_4	0.2658	+0.1263 (+90.5%)
Fe_5C_2	0.1416	-0.0739 (-34.3%)
↓	↓	
Fe_3O_4	0.2658	+0.1242 (+87.7%)

Table 3
BET Surface Area and Pore Volume Data for SiO_2, $MgO•3.75SiO_2$, Al_2O_3 and $MgAl_2O_4$ Supports and $100Fe/6.0Cu/8.1K/260MgAl_2O_4$, $100Fe/6.0Cu/8.1K/250Al_2O_3$, $100Fe/6.0Cu/8.1K/260MgO•3.75SiO_2$ and $100Fe/6.0Cu/8.1K/250SiO_2$ Catalysts

	surface area (m^2g^{-1})	**pore volume (cm^3g^{-1})**
silica	284	1.15
magnesium silicate	231	0.54
alumina	196	0.43
magnesium aluminate	71	0.37
$100Fe/6.0Cu/8.1K/250SiO_2$	127	0.53
$100Fe/6.0Cu/8.1K/260MgO·xSiO_2$	57	0.22
$100Fe/6.0Cu/8.1K/250Al_2O_3$	78	0.19
$100Fe/6.0Cu/8.1K/260MgAl_2O_4$	43	0.16

Table 4
Comparison of FT Activity and Selectivity of Supported Iron Catalysts and Similarly Promoted Precipitated Iron Catalyst

	Supported Catalysts (100Fe/6Cu/8K/250support)			Precipitated
	SiO_2	Al_2O_3	$MgAl_2O_4$	100Fe/3Cu/8K/5SiO_2
Co conversion (mol%)	25	61	62	88
Hydrocarbon rate (g h^1 g-Fe^{-1})	0.17	0.36	0.37	0.51
Water-gas shift $RQ=\frac{[CO_2][H_2]}{[CO][H_2O]}$	3	13	18	25
CO_2 selectivity (C%)	43	48	48	49
H_2/CO usage ratio	0.66	0.54	0.54	0.58
Hydrocarbon selectivity (wt.%)				
C_1	9.0	6.0	4.4	3.6
C_2-C_4 (alkene)	21 (73)	18 (73)	13 (79)	12 (82)
C_5-C_{11} (alkene)	36 (72)	34 (69)	28 (69)	19 (81)
C_{12}+	34	42	54	65

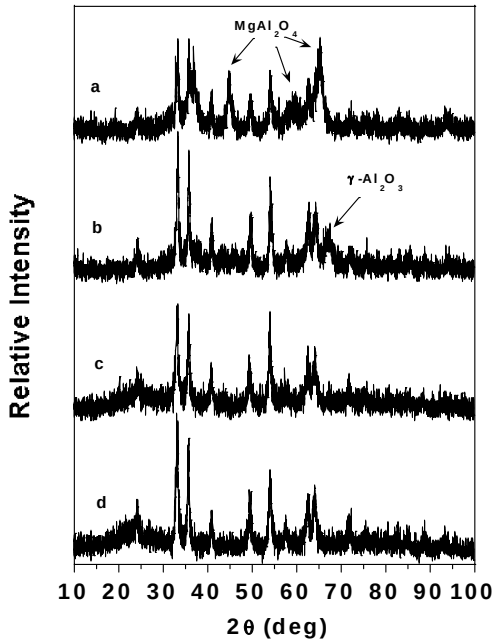

Figure 1. X-ray diffractograms of calcined (a) 100Fe/6.0Cu/8.1K/260$MgAl_2O_4$, (b) 100Fe/6.0Cu/8.1K/250Al_2O_3, (c) 100Fe/6.0Cu/8.1K/260MgO·3.75SiO_2 and (d) 100Fe/6.0Cu/8.1K/250SiO_2.

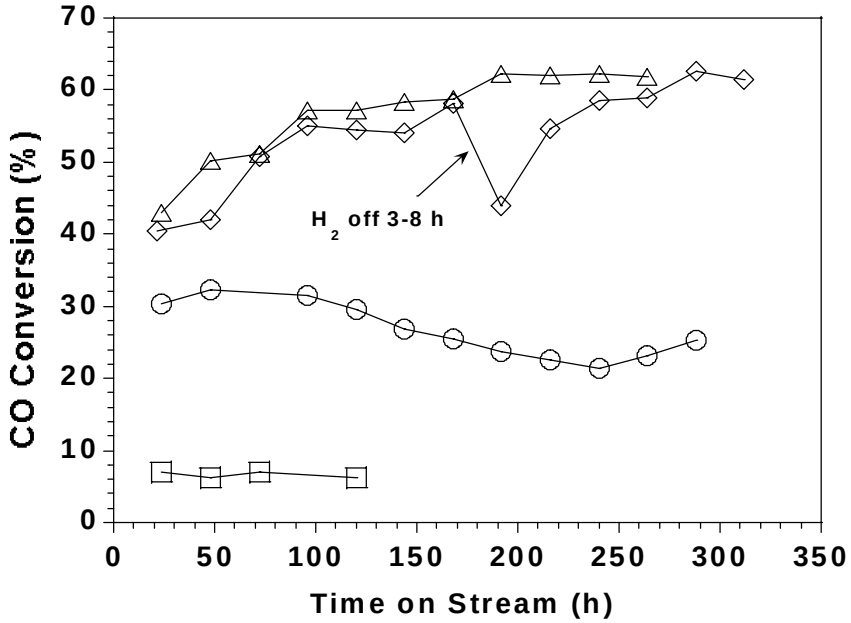

Figure 2. Carbon monoxide conversion as a function of time on stream for (○) 100Fe/6.0Cu/8.1K/250SiO_2, (□) 100Fe/6.0Cu/8.1K/260MgO·3.75SiO_2, (◇) 100Fe/6.0Cu/8.1K/250Al_2O_3 and (△) 100Fe/6.0Cu/8.1K/260$MgAl_2O_4$.

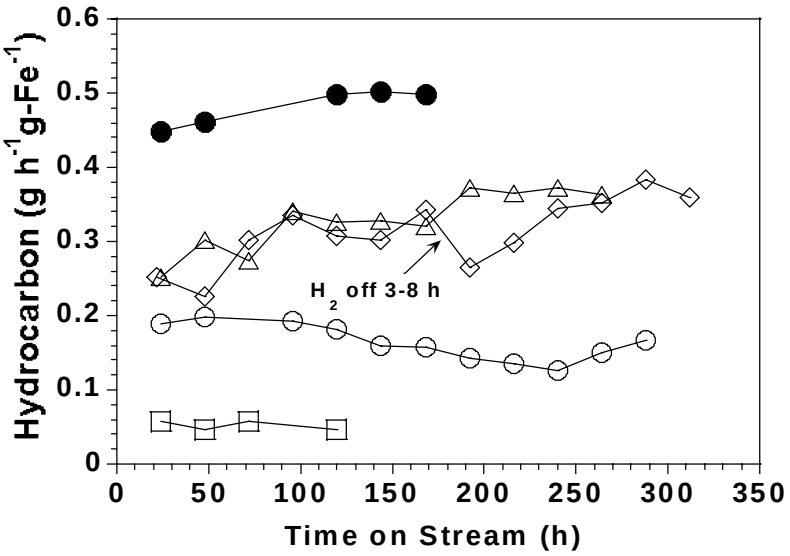

Figure 3. Hydrocarbon production rate on an iron mass basis as a function of time on stream for (○) 100Fe/6.0Cu/8.1K/250SiO_2, (□) 100Fe/6.0Cu/8.1K/260MgO·3.75SiO_2, (◇) 100Fe/6.0Cu/8.1K/250Al_2O_3 (△) 100Fe/6.0Cu/8.1K/260$MgAl_2O_4$ and (●) precipitated 100Fe/6Cu/8K/6SiO_2.

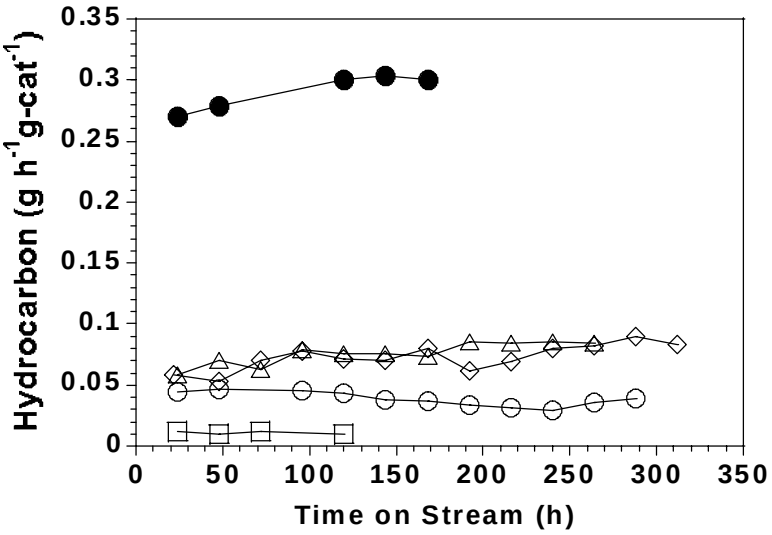

Figure 4. Hydrocarbon production rate on a catalyst mass basis as a function of time on stream for (○) 100Fe/6.0Cu/8.1K/250SiO_2, (□) 100Fe/6.0Cu/8.1K/260MgO·3.75SiO_2, (◇) 100Fe/6.0Cu/8.1K/250Al_2O_3 (△) 100Fe/6.0Cu/8.1K/260$MgAl_2O_4$ and (●) precipitated 100Fe/6Cu/8K/6SiO_2.

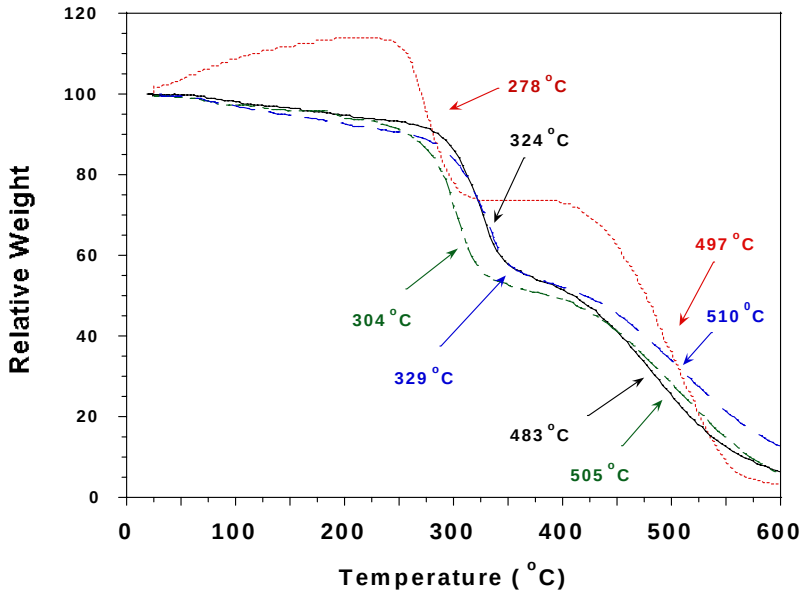

Figure 5. Thermogravimetric analysis with hydogen of (·····)100Fe/6.0Cu/8.1K/250SiO_2, (—) 100Fe/6.0Cu/8.1K/260MgO·3.75SiO_2, (------) 100Fe/6.0Cu/8.1K/250Al_2O_3 (— – —) 100Fe/6.0Cu/8.1K/260$MgAl_2O_4$.

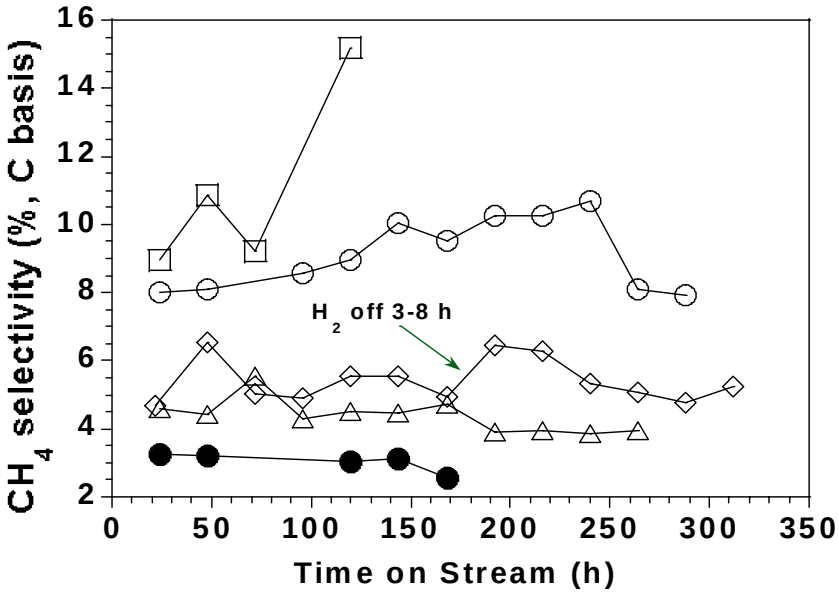

Figure 6. Methane selectivity on an atomic basis of carbon converted to hydrocarbon. (○) 100Fe/6.0Cu/8.1K/250SiO_2, (□) 100Fe/6.0Cu/8.1K/260MgO·3.75SiO_2, (◇) 100Fe/6.0Cu/8.1K/250Al_2O_3 (△) 100Fe/6.0Cu/8.1K/260$MgAl_2O_4$ and (●) precipitated 100Fe/6Cu/8K/6SiO_2.

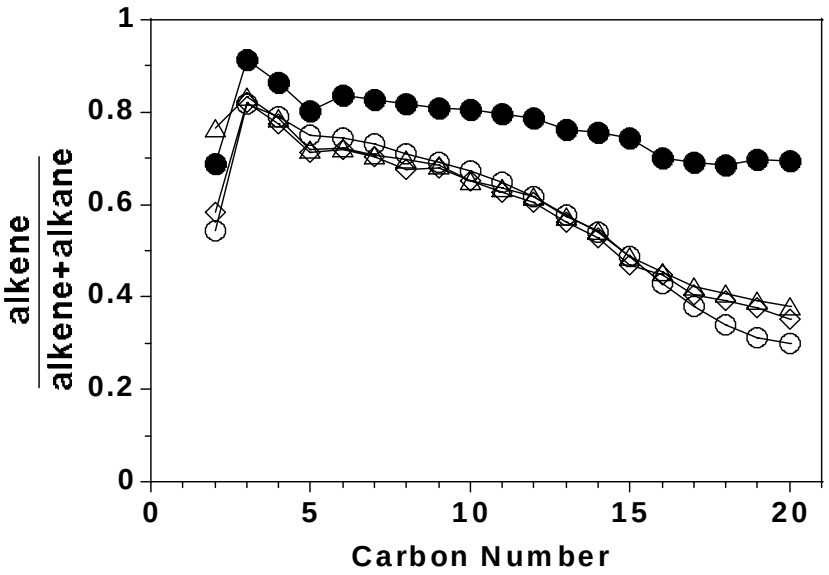

Figure 7. Alkene selectivity as a function of carbon number for (○) 100Fe/6.0Cu/8.1K/250SiO_2, (◇) 100Fe/6.0Cu/8.1K/250Al_2O_3 (△) 100Fe/6.0Cu/8.1K/260$MgAl_2O_4$ and (●) precipitated 100Fe/6Cu/8K/6SiO_2.

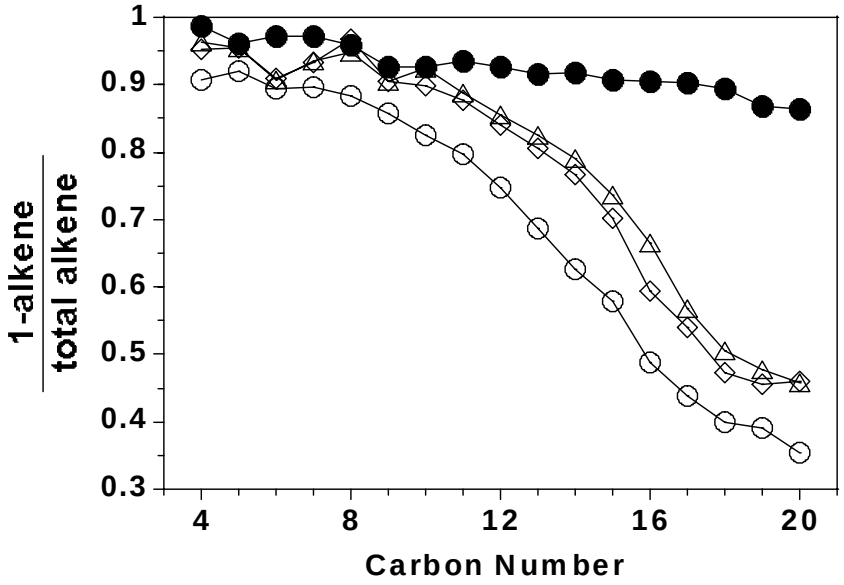

Figure 8. 1-alkene selectivity as a function of carbon number for (○) 100Fe/6.0Cu/8.1K/250SiO_2, (◇) 100Fe/6.0Cu/8.1K/250Al_2O_3 (△) 100Fe/6.0Cu/8.1K/260$MgAl_2O_4$ and (●) precipitated 100Fe/6Cu/8K/6SiO_2.

100Fe/6Cu/8K/250SiO_2 **100Fe/6Cu/8K/260(MgO-3.75SiO_2)**

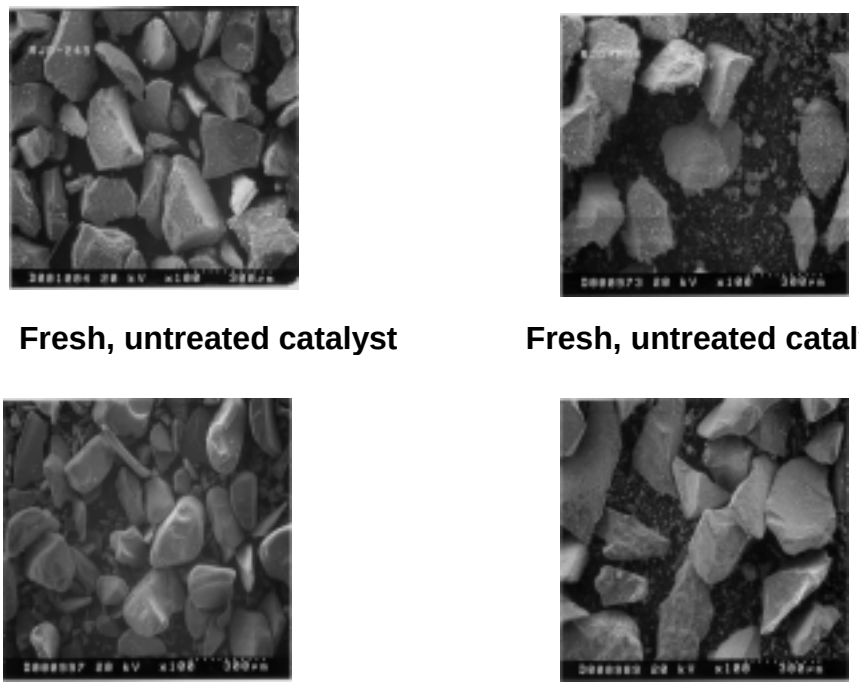

Fresh, untreated catalyst **Fresh, untreated catalyst**

Figure 9. Scanning electron micrographs of the 100Fe/6.0Cu/8.1K/250SiO_2 and 100Fe/6.0Cu/8.1K/260MgO·3.75SiO_2 catalysts before and after FTS.

100Fe/6Cu/8K/250Al_2O_3 100Fe/6Cu/8K/260$MgAl_2O_4$

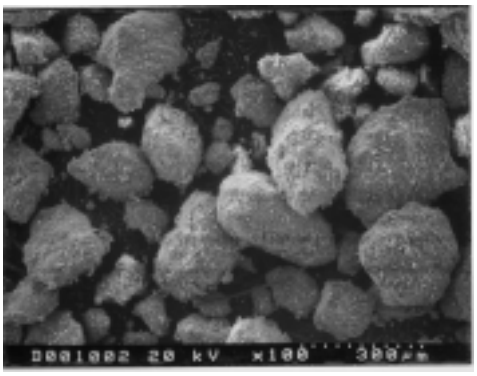

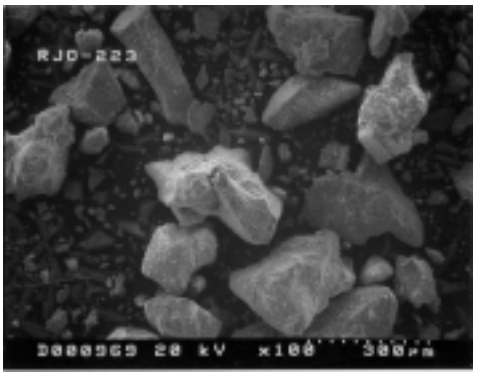

Fresh, untreated catalyst Fresh, untreated catalyst

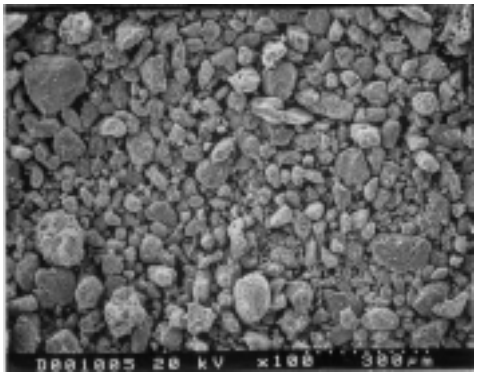

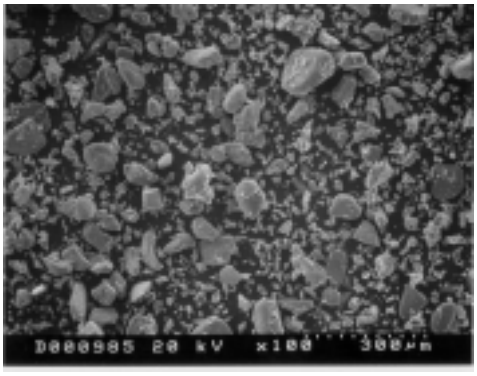

Figure 10. Scanning electron micrographs of the 100Fe/6.0Cu/8.1K/250Al_2O_3 and 100Fe/6.0Cu/8.1K/260$MgAl_2O_4$ catalysts before and after FTS.